Position-sensorless control of permanent-magnet-assisted synchronous reluctance motor

(Article begins on next page)

27 April 2024

Position-Sensorless Control of Permanent-Magnet-Assisted Synchronous Reluctance Motor

Paolo Guglielmi, Michele Pastorelli, Gianmario Pellegrino, and Alfredo Vagati, *Fellow, IEEE*

Abstract—The sensorless control of permanent-magnet-assisted synchronous reluctance (PMASR) motors is investigated, in order to conjugate the advantages of the sensorless control with full exploitation of the allowed operating area, for a given inverter. An additional pulsating flux is injected in the *d*-axis direction at low and zero speed, while it is dropped out, at large speed, to save voltage and additional loss. A flux-observer-based control scheme is used, which includes an accurate knowledge of the motor magnetic behavior. This leads, in general, to good robustness against load variations, by counteracting the magnetic cross saturation effect. Moreover, it allows an easy and effective correspondence between the wanted torque and flux and the set values of the chosen control variables, that is *d*-axis flux and *q*-axis current. Experimental verification of the proposed method is given, both steady-state and dynamic performance are outlined. A prototype PMASR motor will be used to this aim, as part of a purposely assembled prototype drive, for light traction application (electric scooter).

Index Terms—Permanent-magnet-assisted synchronous reluctance (PMASR) motor, sensorless control.

I. INTRODUCTION

IN THE FIELD of controlled drives, adoption of motors of the synchronous type is continuously increasing. This is related to many reasons, such as the better efficiency, the "cold rotor" prerogative, the better torque-to-inertia values, etc. Typically, permanent-magnet (PM) excited motors are used, while the surface-mounted (isotropic) rotor represents the most common design choice. However, for the applications where a large constant-power speed range is required (e.g., spindle drives, traction drives, etc.), the surface-mounted rotor does not represent a good choice. In fact, a tradeoff has to be found, between the rated torque performance and the flux-weakening capability [10]. An appropriate solution, in this case, would be a suitably designed interior PM (IPM) motor.

This topic has received adequate attention in the literature since the 1980s [1], [2]. However, the former IPM designs were mainly PM machines, with a minor contribution from the reluctance torque. On the contrary, [4], [5], and [7] have shown that the best design choice for flux-weakening performance leads to a machine with good saliency, thus minimizing the PM. content and the consequent need for large demagnetizing currents. In this case, the IPM machine could be more properly called a PM-assisted synchronous reluctance (PMASR) machine. The work in [4] must be mentioned, in particular, where a nice generalization of the problem is presented, introducing the per-unit "saliency versus magnet" plane and pointing out all the possible types of machine designs. Among them, the ones leading to a PMASR machine are shown to be preferable, since they are suited to wide constant-power speed ranges.

On the other hand, a machine with a good saliency is also desirable from another point of view, that is, its suitability to sensorless control. The removal of any shaft transducer is desired in a very broad class of practical applications, for well-known reasons including lower cost and reduced motor size. Moreover, in the last few years the search for position-sensorless position control has emerged, thus involving zero-speed operation at a predetermined rotor position. The possible application field is very wide, from many kinds of position control to those speed controls where extreme speed accuracy is wanted. As a consequence, a shift of interest is justified from induction motors to synchronous ones and, among them, to those showing a good anisotropic behavior, i.e., synchronous reluctance and PMASR machines. In fact, a good saliency always allows, at low speed, the rotor position estimation, independently of the chosen method of excitation (e.g., injection of high-frequency additional fields, various types of modified pulsewidth-modulation (PWM) techniques, etc.). Because of the above reasons, sensorless control of IPM machines is becoming a much-frequented topic, in the literature. In this paper, the control peculiarities of PMASR machines are pointed out, giving evidence to the allowed operating area (AOA) in the state plane. Then, a sensorless control scheme is proposed, which was shown to be very effective for synchronous reluctance motors [8]. Lastly, experimental results are given, as obtained from a prototype drive, adopting a prototype PMASR motor.

II. MACHINE PERFORMANCE AND CONTROL LIMITS

Let us start from consideration of the measured flux–current relationship (Fig. 1) of the PMASR machine adopted in the experiments, that is, a motor for scooter application having 20 N·m as rated torque (Fig. 2). The machine stator diameter is 150 mm and its core length is 142 mm, the rotor inertia is $4.5 \cdot 10^{-3} \ \mathrm{kg \cdot m^2}$.
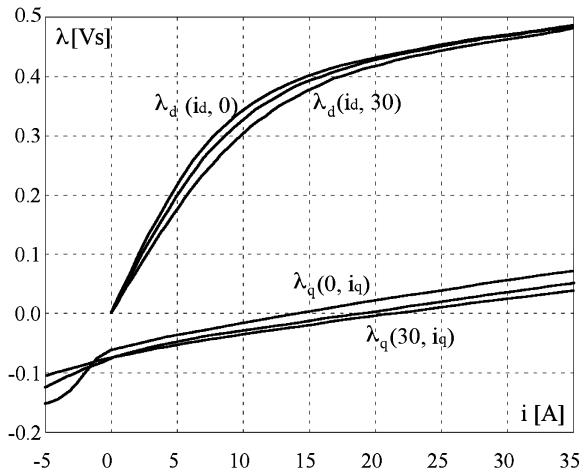
Fig. 1. $\lambda_d(i_d, i_q)$ and $\lambda_d(i_d, i_q)$ versus current, measured for $i_d, i_q = 0, 15, 30$ A.

Fig. 2.   Rotor and stator layout.

Fig. 3.   Current and flux vectors.

Fig. 4.   AOA of current vector (positive torque).
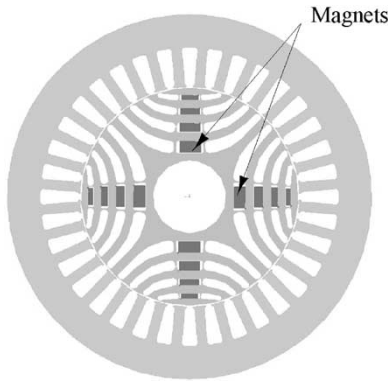
The Fig. 1 characteristics refer to a (d, q) frame synchronous to the rotor, with the d axis aligned to the direction of maximum permeance. This looks unusual, when dealing with PM motors. However, since we deal with a PMASR motor, the main flux component lies on the d axis, because of the fairly good anisotropic behavior (the unsaturated anisotropy ratio is larger than ten). This was obtained by a four-barrier-per-pole rotor structure (Fig. 2), filled with NdFeB magnets. From Fig. 1 characteristics we can observe the following.

- Both d- and q-axes behaviors are nonlinear, in principle: a cross-saturation effect is evident, also.
- The differential anisotropy is quite good, for the usual working points: however, it tends to disappear, when the d axis is put into deep saturation.
- The effect of cross-saturation on the q component of flux is comparable to that due to the thermal drift of the magnets.

A simple linearity between flux and current cannot be assumed. However, a simplified model could be adopted, as suggested in [5]. A linear relationship was assumed there for the q axis ($L_q = \text{const}$), while the d axis was described by the apparent $L_d(i_d)$ and differential $L_{dd}(i_d)$ inductances, which are, of course, related to each other. The cross saturation was neglected. The result there obtained was a general (parametric) definition o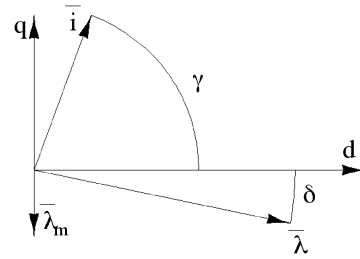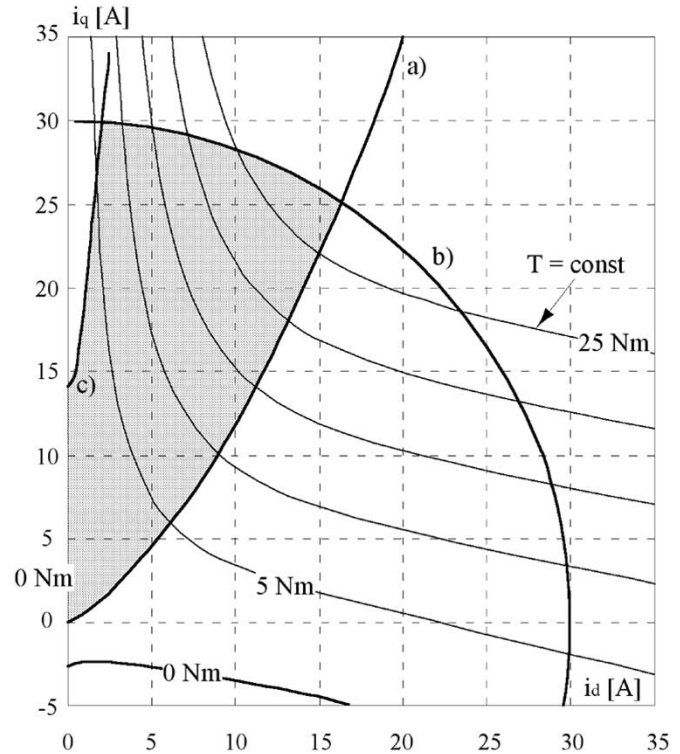f the allowed operating area (AOA) during flux weakening, once voltage and current limitations are provided by the inverter.

On the other hand, from motor characteristics like those in Fig. 1 the AOA can be directly obtained, for control purposes. With reference to the (d, q) frame previously introduced, current and flux vectors can be defined by their d, q component or, alternatively, by their modules i, λ and their arguments γ, δ, respectively, as summarized in Fig. 3, where the flux λ_m due to PMs is also evidenced.

The AOA for the current vector (positive torque) is shown in Fig. 4 (shaded). In general, three different curves can be recognized. First $a)$, the $k_{T\,\max}$ locus (max N·m/A at fixed current amplitude), which represents a common control choice in the constant-torque region. Then, the current limitation during flux weakening $b)$ moves the current vector toward the q axis, until the locus $c)$ of maximum torque with constrained voltage is eventually reached. Along this locus the current vector is definitely reduced, up to the point at which the total flux would be zero, thus corresponding to infinite speed. The AOA for negative torque is symmetrical, with respect to the q axis.
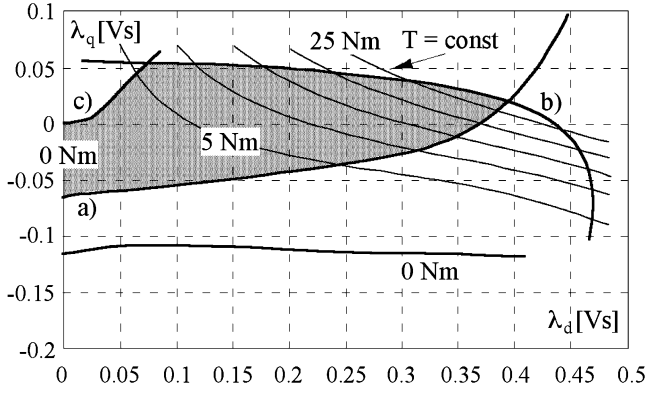
Fig. 5.   AOA of flux vector (positive torque).

Fig. 6.   Machine control structure.

In synthesis, the three zones can be defined as shown by (1), V_s and I_s being the maximum allowed phase voltage and current amplitudes.

Fig. 5 shows the AOA in the flux plane (λ_d, λ_q), where the three zones *a)*, *b)*, and *c)* are still pointed out

$$\begin{cases} zone\ a): & \frac{\partial T}{\partial \gamma} = 0 \\ zone\ b): & i = I_s, \quad v = V_s \\ zone\ c); & \frac{\partial T}{\partial \delta} = 0, \quad v = V_s. \end{cases} \tag{1}$$

If $L_q I_s = \lambda_m$, the limit situation occurs for which the maximum current I_s can flow at infinite speed (at unity power factor) [2]–[5], [9]. In this case the *c)* zone disappears.

As seen, the allowed drive working points can be described by any combination of current or flux components. However, a different performance is obtained depending on the two variables to be controlled directly (control variables). The most common choice is (i_d, i_q), since currents are measured quantities. However, Fig. 4 points out the large sensitivity of this choice to the errors on the measurement/estimation of the synchronous frame position at high speed, when i_d gets very low values. On the other hand, the opposite choice (λ_d, λ_q) would be much sensitive to the uncertainty of the q-axis model. A best choice seems to be (λ_d, i_q), which looks the most robust, at least at load, when λ_d and i_q represent the largest components. However, an increased sensitivity to errors would occur at no load, when the $\lambda_q i_d$ term is important, in the torque equation: this can lead to loss of control in case of sensorless control, as mentioned in the following.

A completely different choice of control variables was made in [3], [6], where a flux-oriented control frame was chosen for a control of the sensored type. In this way, a good robustness was obtained at the expense of lower dynamics.

The block scheme of the (λ_d, i_q)-based machine control structure is shown in Fig. 6. $A(\vartheta)$ represents the rotation matrix. The motor currents are measured, while the motor voltages are obtained from dc bus measurement and knowledge of the inverter states.

The key role is played by the observer block, which must provide the observed d-flux component for flux feedback, together with the rotor observed position (and speed). The additional, high-frequency flux signal λ_{di} is also shown, which is nee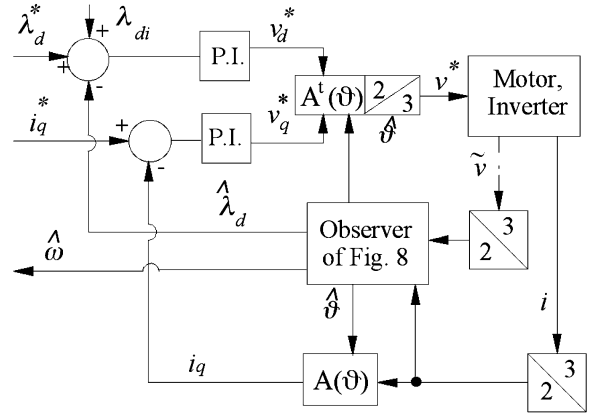ded, at low and zero motor speed, for sensorless operation. The set flux λ_d^* and current i_d^* values can be obtained from the set torque and flux amplitude (or speed), as shown in the following.

III. SENSORLESS OPERATION

At high speed (frequency) the flux linkage can be easily estimated by voltage integration, thus allowing sensorless operation. However, when torque control at zero speed is required, the flux estimation comes from knowledge of the flux–current relationship (magnetic model, Fig. 1) and the rotor position is obtained by tracking the rotor saliency. Let us observe that all the commonly adopted saliency-based methods refer to the "differential saliency" behavior of the machine. For this reason, synchronous reluctance and PMASR motors behave in a similar way, since they are both described by similar differential inductances. For equivalent rotor designs, magnet embedding will even improve the anisotropy, at high load. For the above reasons, the method already proposed by the authors [8] for synchronous reluctance motors is here adopted for a PMASR motor.

A peculiarity of this method is to be robust against cross-saturation. It has been shown in [8] that cross saturation introduces a displacement of the backward component due to saliency, thus leading to a relevant error in the position estimate. As an example, the (2) can be written, relating the differential phasors $\delta\lambda_{dq}$ and δi_{dq} to each other ($\delta i'_{dq}$ is the complex conjugate): l_d, l_q, l_{dq} are the differential inductances $(\partial\lambda_d/\partial i_d)$, $(\partial\lambda_q/\partial i_q)$, $(\partial\lambda_d/\partial i_q) = (\partial\lambda_q/\partial i_d)$, respectively,

$$\delta\lambda_{dq} = \frac{l_d + l_q}{2}\delta i_{dq} + \left(\frac{l_d - l_q}{2} + j l_{dq}\right)\delta i'_{dq}. \tag{2}$$

As can be seen, the backward coefficient is complex, due to the l_{dq} term. Equation (2) refers to current excitation and flux detection; however, the same effect arises when flux (voltage) is injected and current is detected, which is more common in the literature.

In the proposed method the above-cited problem is overcome, because a flux-observer structure is used and flux signals are both injected and detected. The flux–current relationship (Fig. 1) is included in the flux-observer structure shown in Fig. 7, represented by the nonlinear block L. As stated, $A(\vartheta)$ is the rotation matrix, from stationary (α, β) to synchronous (d, q) frame. The gain matrix is reduced to a scalar, g, for simplicity.
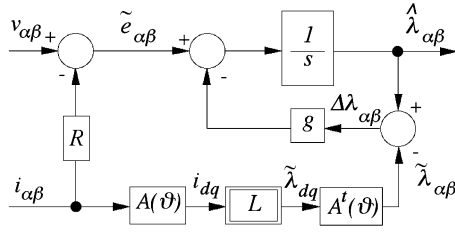
Fig. 7.   Flux observer structure.

Fig. 8.   Suggested sensorless observer.

The dynamic behavior of this flux observer is pointed out by (3), in terms of Laplace transfer functions. As can be seen, the voltage integral $\lambda_{\alpha\beta} = (v_{\alpha\beta} - Ri_{\alpha\beta})/s$ is high-pass filtered, while the flux estimate from the magnetic model $\tilde{\lambda}_{\alpha\beta}$ is low-pass filtered. As a consequence, they both work at the best, since voltage integration fails at low frequency while the magnetic behavior is affected, at high frequency, by core losses

$$\hat{\lambda}_{\alpha\beta} = \frac{s}{s+g}\frac{v_{\alpha\beta} - Ri_{\alpha\beta}}{s} + \frac{g}{s+g}\tilde{\lambda}_{\alpha\beta}. \qquad (3)$$

The choice of g (cros-over pulsation) is a matter of tradeoff between these two types of error, taking into account that the motor voltage is estimated from dc bus voltage and inverter states.

The scheme of Fig. 7 requires knowledge of the rotor angle ϑ. However, at high frequency, when the estimated flux $\hat{\lambda}_{\alpha\beta}$ is mainly dependent on voltage integration, the ϑ angle should be self-supplied to the observer, coming from vector and dot products between the observed flux on the stationary frame $\hat{\lambda}_{\alpha\beta}$ and the estimated one on the synchronous frame $\tilde{\lambda}_{\alpha\beta}$. In practice, (4) can be used. They are also effective during fast flux transients, since in this case the electromotive force (EMF) signal is large

$$\sin\tilde{\vartheta} = \frac{\tilde{\lambda}_{dq} \wedge \hat{\lambda}_{\alpha\beta}}{\lambda^2} \quad \cos\tilde{\vartheta} = \frac{\tilde{\lambda}_{dq} \times \hat{\lambda}_{\alpha\beta}}{\lambda^2}. \qquad (4)$$

Of course, at steady state and low speed, the observed flux tends to the one estimated from the block L and, consequently, the angle $\tilde{\vartheta}$ estimated by (4) becomes meaningless. This is clearly shown by (5), which is easily obtained from (3). The flux $\lambda_{\alpha\beta}$ represents the true one, as ideally obtained from EMF integration. At steady state, the difference between estimated and observed fluxes vanishes; thus, (4) can be satisfied by any value of $\tilde{\vartheta}$. As a consequence, since a controlled behavior is wanted at low and zero speed, a saliency-tracking loop has to be added, to the flux observer scheme of Fig. 7. The proposed solution is shown in Fig. 8

$$\Delta\lambda_{\alpha\beta} = \hat{\lambda}_{\alpha\beta} - \tilde{\lambda}_{\alpha\beta} = \frac{s}{s+g}\left(\lambda_{\alpha\beta} - \tilde{\lambda}_{\alpha\beta}\right). \qquad (5)$$

A high-frequency sinusoidal signal λ_{di} is injected, in the estimated d-axis direction, in addition to the motor reference flux. As a misalignment indicator, the q component of the flux error $\Delta\lambda$ shown in Fig. 7 is used. Thus, the errors due to cross saturation, as discussed above, are here inherently compensated by the inclusion of the magnetic model L in the Fig. 7 observer. Note that the high-frequency q components of both the true (λ_q) and the estimated $(\tilde{\lambda}_q)$ fluxes vanish, for correct orientation. Their
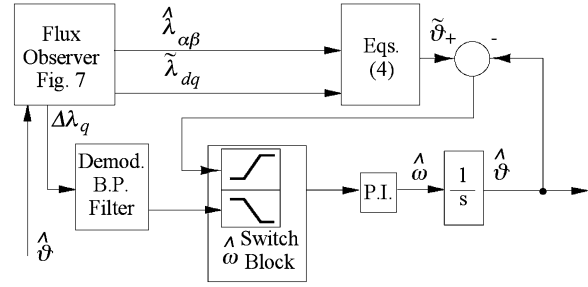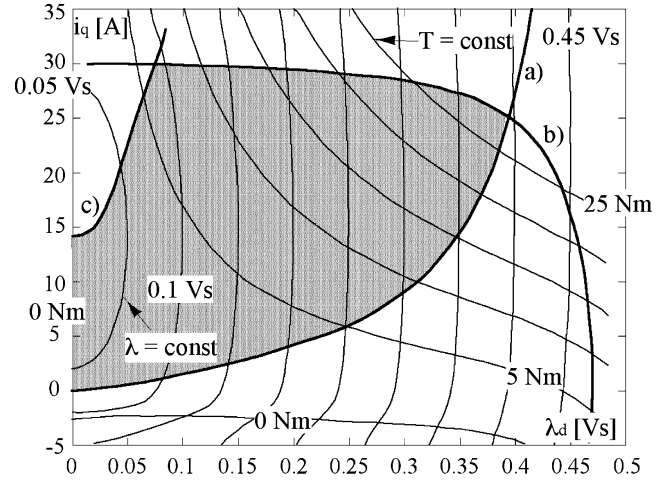

Fig. 9.   Constant-torque and constant-flux loci in the (λ_d, i_q) plane.

difference $(\Delta\lambda_q)$ has been used as representative of the position error, because it is inherently high-pass filtered, owing to (5).

In the Fig. 8 scheme, the high-frequency $\Delta\lambda_q$ error, once demodulated, is fed to the proportional–integral (PI) regulator through a weighting function which has unitary value at low speed and zero value at high speed.

The output of the PI regulator is integrated and then compared with the result of (4). The difference between $\tilde{\vartheta}$ and $\hat{\vartheta}$ is also used as error in the tracking loop, combined with the previous one, depending on the speed. At high speed, when the EMF is a reliable signal and the flux injection is dropped out, the result of (4) is directly sent to the PI regulator and then integrated. The weighting functions of the "switch" block move linearly from one to zero and vice-versa. The shapes of the weighting functions are related to the value of the flux observer gain and to the point when the flux injection is dropped out. The choice of the weighting functions is definitely made in order to reduce the resulting noise content. The signal $\hat{\omega}$ is used as speed feedback for the speed loop.

IV. TORQUE AND SPEED CONTROL

As stated above, the control variables (λ_d, i_q) must be set from the requested torque T^* and flux amplitude λ^*, which in turn depends on the speed value. In order to fix the reference λ_d and i_q values a lookup table with reference torque and speed as input quantities can be used. In Fig. 9 the usual *a)*, *b)*, and *c)* loci are shown in the λ_d, i_q plane, together with the constant torque and constant flux loci. An assigned torque value can be
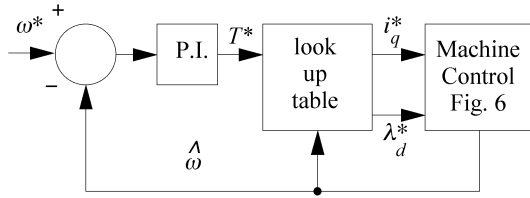
Fig. 10.   General control scheme.

obtained by several couples of (λ_d, i_q) values, that implies different flux values. If a constant torque at variable speed is required the motor working point can move along the constant torque locus in order to reach the limit of the AOA. Then the AOA limit is tracked if the flux is furtherly decreased. The general control scheme is summarized in Fig. 10.

V. EXPERIMENTAL RESULTS

Based on the previously described control scheme, a prototype sensorless drive has been assembled and tested.

An insulated-gate-bipolar-transistor (IGBT)-based 535-V supplied inverter was used, PWM operated at a 10-kHz frequency. The adopted digital signal processor (DSP) was an ADSP-21 020 (input clock 33 MHz) installed on the original evaluation board. The analog inputs (motor currents and dc-bus voltage) were synchronously sampled at PWM frequency (10 kHz), by 12-bit A/D converters. The currents were transduced by a Hall-effect CT, while the dc voltage was acquired by a differential amplifier. The actual motor position and speed are measured by an incremental encoder. The described angle detection scheme bases its performance on the differential saliencies. However, since permanent magnets are present in the machine, at the startup the system has to detect the magnet polarity, in order to set the correct initial value of the angle. In order to cope with this problem a start up procedure has been adopted, based on the value of the apparent inductance. Before enabling current and flux control loops, the motor is supplied with a balanced three phase system (100 V peak) at 300-Hz frequency and the motor currents are detected. When the current is aligned with the q axis the motor shows a low apparent inductance, that leads to a peak in the current amplitude. However peaks of different amplitude occur when q or $-q$ directions are excited as shown in Fig. 11.

This allows an easy detection of the magnet polarity, since the highest peak occurs when the current is in the same direction of the PM flux $(-q)$.

In order to prove the effectiveness of the proposed method the PMASR motor has been driven by an auxiliary motor, while the startup procedure was operating. The sine of the detected angle $(\sin\vartheta_0)$ is shown in Fig. 12 together with the sine of the actual angle $(\sin\vartheta)$. The performance of Fig. 12 looks satisfactory. It can be noted that the detected angle shows a large quantization noise: this represents an acceptable trade off between the time needed to initialize the control and the accuracy, since this startup procedure has the only target to give an initial angle value to the sensorless control.

The behavior of the complete sensorless control scheme is shown in the following experimental results, for which a simple
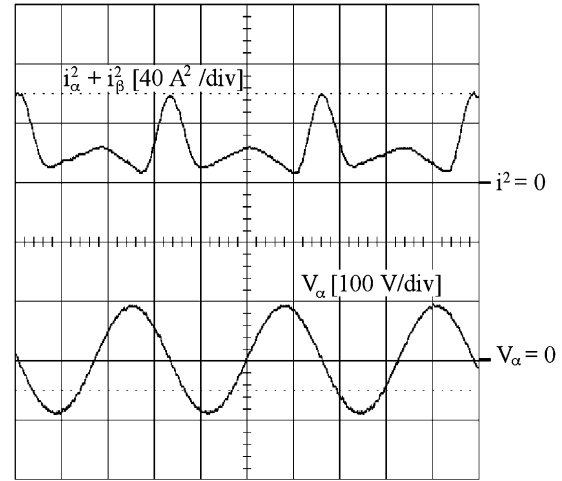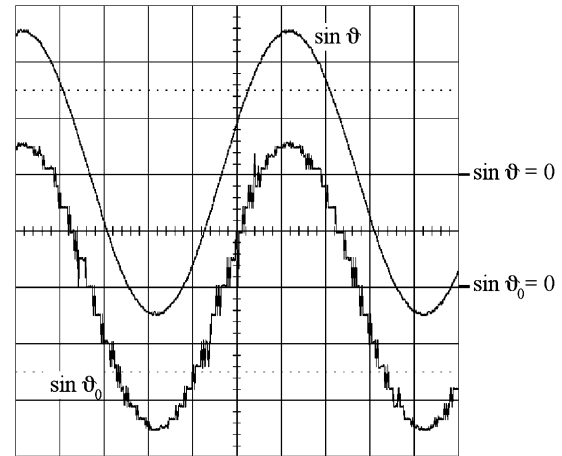

Fig. 11.   Excitation voltage V_α and squared input current amplitude for the angle detection at startup. Time base: 1 ms/div.

Fig. 12.   Performance of the startup detection method. Time base: 500 ms/div.

reference generation law has been adopted. Both $\lambda_d{}^*$ and $i_q{}^*$ are set equal to zero when the required torque is zero, while at the maximum torque of 25-N·m flux and current references have been fixed on the maximum N·m/A locus. At intermediate torque values both $\lambda_d{}^*$ and $i_q{}^*$ are linear functions of the torque.

This flux-weakening profile does not represent the best choice since a better solution would be to follow the constant torque locus as long as possible inside the AOA (Fig. 9). However, this control strategy, which is optimal for a sensored control, has lead to instability in the sensorless case.

In the adopted flux weakening profile the torque is reduced starting from 350 rad/s, which is immediately after the border of the flux injection region.

In Fig. 13, a complete startup transient is shown, from 0 to 100 rad/s. The motor has been purposely set in a large error position with respect to the initial one in the DSP, and than let free to run. The fast convergence of the error and the consequent startup delay (10 ms) can be appreciated. After this a step transient is imposed and full torque is given. It can be seen that the angle accuracy is good all over the speed transient.

In Figs. 14 and 15, two different step transients from -500 to $+500$ rad/s and from -800 to $+800$ rad/s are shown. Both measured and estimated speed are presented showing a very

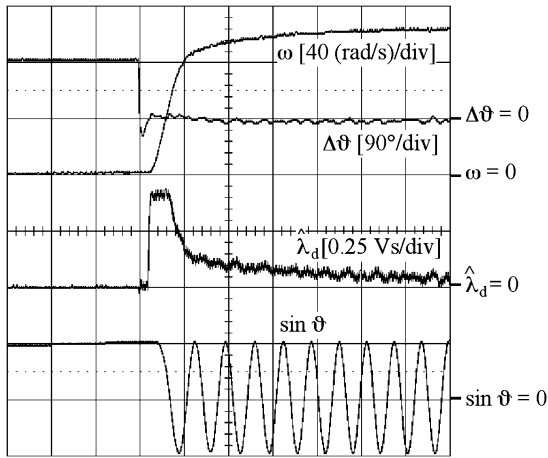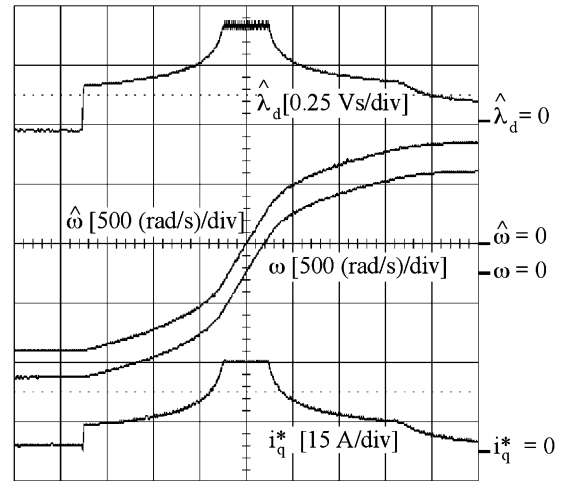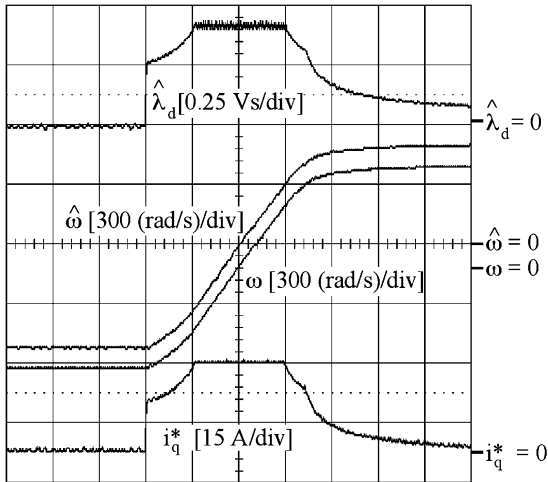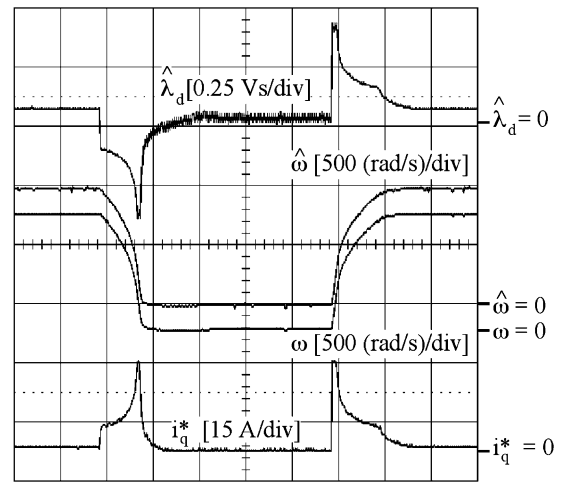Fig. 13.   First start after the turn-on. Time base: 50 ms/div.

Fig. 14.   ±500 rad/s step transient. Time base: 100 ms/div.

Fig. 15.   ±800 rad/s step transient. Time base: 200 ms/div.

Fig. 16.   ±950 rad/s step transient. Time base: 1 s/div.

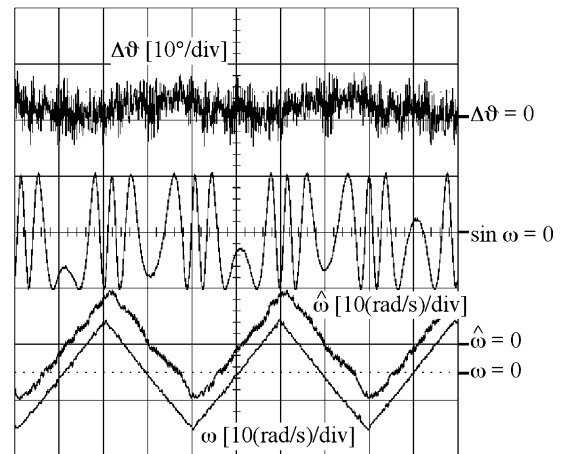Fig. 17.   Triangular speed response (0.25 Hz, ±10 rad/s). Time base: 1 s/div.

good agreement between them. The controlled flux and the reference i_q current are also given in order to show the adopted reference generation scheme and the performance of the control speed loop. Both flux and current are weakened beyond the base speed to avoid stability problems, as stated.

The maximum acceleration is 3000 rad/s^2, with a total inertia (motor + load) of $6.5 \cdot 10^{-3}$ kg · m^2.

In Fig. 16 a stop and go from 9000 r/min down to zero and than up to 9000 r/min is given, showing the performance with positive and negative torque requirements, at zero speed and very high speed as well.

Triangular and sinusoidal speed references are presented in Figs. 17 and 18 showing the performance of the speed loop and the reasonable accuracy of the method, since the estimated angle error is fairly limited.

Finally, a load step response is presented in Fig. 19, where the motor has been connected to an auxiliary torque controlled motor, and a near-to-rated torque is applied. The estimated and real speeds show good accordance. The recovery time is consistent with the actual speed bandwidth. The observed d flux and q motor current are also reported. They are both affected by the high-frequency injection signal λ_{di} (800 Hz, 0.02 V·s peak).

VI. CONCLUSION

A sensorless control for a PMASR motor has been presented. The obtained performance shows a quite large flux-weakening range together with fairly good dynamics and accuracy. Moreover, the control is sufficiently robust for a large range of load
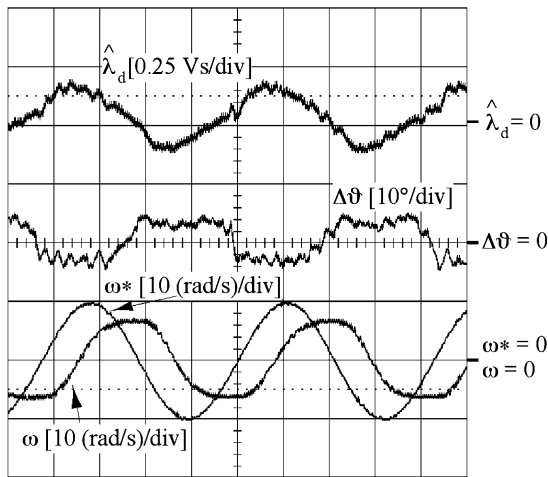
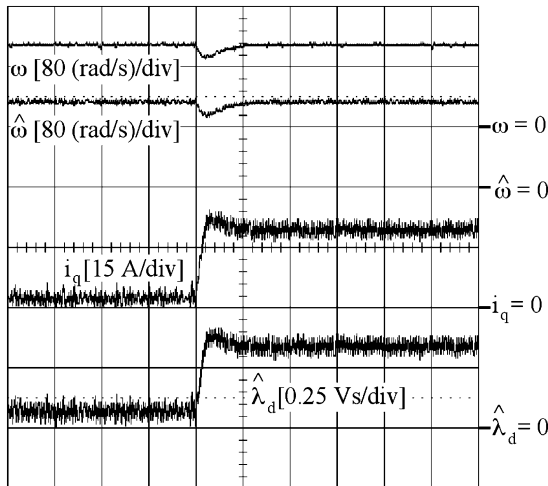Fig. 18. Sinusoidal speed response (5 Hz, ±10 rad/s). Time base: 50 ms/div.

Fig. 19. Step load response at 100 rad/s. Time base: 500 ms/div.

and speed while a good zero-speed behavior is obtained. A weak point still regards the no-load performance, depending on the quite small value of the PM flux; further improvements are possible on this point. Moreover, some work is still needed for better exploitation of the AOA during flux weakening.

REFERENCES

[1] T. M. Jahns, "Flux-weakening regime operation of an interior permanent magnet synchronous motor drive," *IEEE Trans. Ind. Applicat.*, vol. IA-23, pp. 681–689, July/Aug. 1987.

[2] R. F. Schiferl and T. A. Lipo, "Power capability of salient pole permanent magnet synchronous motors in variable speed drive applications," *IEEE Trans. Ind. Applicat.*, vol. 26, pp. 115–123, Jan.–Feb. 1990.

[3] M. Bilewski, L. Giordano, A. Fratta, A. Vagati, and F. Villata, "Control of high performance interior permanent magnet synchronous drives," *IEEE Trans. Ind. Applicat.*, vol. 29, pp. 328–337, Mar./Apr. 1993.

[4] W. L. Soong and T. J. E. Miller, "Field-weakening performance of brushless synchronous AC motor drives," in *Proc. IEE—Elect. Power Applicat.*, vol. 141, Nov. 1994, pp. 331–340.

[5] A. Fratta, A. Vagati, and F. Villata, "Permanent magnet assisted synchronous reluctance drives: drive power limits," in *Proc. PCIM'92*, Nuremberg, Germany, Apr. 27–30, 1992, pp. 196–203.

[6] ——, "Permanent magnet assisted synchronous reluctance drives: Comparative analysis of control requirements," in *Proc. PCIM'92*, Nuremberg, Germany, Apr. 27–30, 1992, pp. 187–195.

[7] T. M. Jahns, "Component rating requirements for wide constant power operation of interior pm synchronous machine drives," in *Conf. Rec. IEEE-IAS Annu. Meeting*, vol. 3, 2000, pp. 1697–1704.

[8] A. Vagati, M. Pastorelli, P. Guglielmi, and E. Capecchi, "Position sensorless control of transverse-laminated synchronous reluctance motors," *IEEE Trans. Ind. Applicat.*, vol. 37, pp. 1176–1768, Nov./Dec. 2001.

[9] S. Morimoto, Y. Takeda, T. Hirasa, and K. Taniguchi, "Expansion of operating limits for permanent magnet motor by current vector control considering inverter capacity," *IEEE Trans. Ind. Applicat.*, vol. 26, pp. 866–871, Sept./Oct. 1990.

[10] B. J. Chalmers, L. Musala, and D. F. Gosden, "Performance characteristics of synchronous motor drives with surface magnets and field weakening," in *Conf. Rec. IEEE-IAS Annu. Meeting*, San Diego, CA, 1996, pp. 511–517.

[11] J.-I.Jung-Ik Ha, K.K. Ide, T. Sawa, and S.-K.Seung-Ki Sul, "Sensorless position control and initial position estimation of an interior permanent magnet motor," in *Conf. Rec. IEEE-IAS Annu. Meeting*, vol. 4, 2001, pp. 2607–2613.

[12] M. Schroedl, "Sensorless control of AC machine at low speed and standstill based on the 'INFORM' method," in *Conf. Rec. IEEE-IAS Annu. Meeting*, 1996, pp. 270–277.

[13] S. Ogasawara and H. Akagi, "Implementation and position control performance of a position-sensorless IPM motor drive system based on magnetic saliency," *IEEE Trans. Ind. Applicat.*, vol. 34, pp. 806–812, July/Aug. 1998.

[14] P. L. Jansen and R. D. Lorenz, "Transducerless position and velocity estimation in induction and salient AC machines," *IEEE Trans. Ind. Applicat.*, vol. 31, pp. 240–247, Mar./Apr. 1995.

Paolo Guglielmi was born in Imperia, Italy, in 1970. He received the M.Sc. degree in electronic engineering and the Ph.D. degree in electrical engineering from the Politecnico di Torino, Turin, Italy, in 1996 and 2001, respectively.

In 1997, he joined the Department of Electrical Engineering, Politecnico di Torino, where he became a Researcher in 2002. His fields of interest are power electronics, high-performance servo drives, and computer-aided design of electrical machines. He has authored several papers published in technical journals and conference proceedings.

Dr. Guglielmi is a Registered Professional Engineer in Italy.

Michele Pastorelli was born in Novara, Italy, in 1962. He received the Laurea and Ph.D. degrees in electrical engineering from the Politecnico di Torino, Turin, Italy, in 1987 and 1992, respectively.

In 1988, he joined the Department of Electrical Engineering, Politecnico di Torino, where he is currently an Associate Professor. His fields of interest include power electronics, high-performance servo drives, and energetic behaviors of electrical machines. He has authored about 70 papers published in technical journals and conference proceedings.

Dr. Pastorelli is a Registered Professional Engineer in Italy.

Gianmario Pellegrino was born in Turin, Italy, in 1973. He received the M.Sc. and PhD. degrees in electrical engineering from the Politecnico di Torino, Turin, Italy, in 1998 and 2002, respectively.

In 2002, he was a Guest Researcher at Aalborg University, Denmark, working for Sauer Danfoss. He is presently a Researcher at the Politecnico di Torino, working in the fields of power electronics, high-performance servo drives, and electrical machines design. He has authored several papers published in technical journals and conference proceedings.

Dr. Pellegrino is a Registered Professional Engineer in Italy.

Alfredo Vagati (M'87–F'98) received the Laurea degree in electrical engineering from the Politecnico di Torino, Turin, Italy, in 1970.

After a few years working in industry with Olivetti, he joined the Politecnico di Torino in 1975 as Assistant Professor. From 1982 to 1990, he was an Associate Professor of Electrical Drives In 1990, he became a Professor of Electrical Machines and Drives at the University of Cagliari, Italy In 1991, he rejoined the Politecnico di Torino in the same capacity. He was Chair of the Electrical Engineering Department of the Politecnico di Torino from 1995 to 2003. His scientific activity, in the field of electrical machines and drives, has particularly concerned high-performance ac drives. He has been involved in several industrial projects, in the field of ac drives, as both a designer and a scientific reference. The most important activity of this kind has concerned design and control of newly developed, high-performance synchronous reluctance motors. He has led several country-wide and European research projects, in the field of design and control of synchronous-machine-based drives, for different applications, including home appliances and the automotive world. He has authored or coauthored more than 80 technical papers.

Prof. Vagati is a permanent member of the Technical Program Committee of the PCIM International Conference and Exhibition. He is also a member of the Industrial Drives and Electric Machines Committees of the IEEE Industry Applications Society.